

Building Lightweight Semantic Segmentation Models for Aerial Images Using Dual Relation Distillation

Minglong Li^a, Lianlei Shan^a, Weiqiang Wang^{a,*}, Ke Lv^b, Bin Luo^c, Si-Bao Chen^c

^a*School of Computer Science and Technology, University of Chinese Academy of Sciences, Beijing, China*

^b*School of Engineering Science, University of Chinese Academy of Sciences, Beijing, China*

^c*MOE Key Lab of Signal Processing and Intelligent Computing, School of Computer Science and Technology, Anhui University, Hefei, China*

Abstract

Recently, there have been significant improvements in the accuracy of CNN models for semantic segmentation. However, these models are often heavy and suffer from low inference speed, which limits their practical application. To address this issue, knowledge distillation has emerged as a promising approach to achieve a good trade-off between segmentation accuracy and efficiency. In this paper, we propose a novel dual relation distillation (DRD) technique that transfers both spatial and channel relations in feature maps from a cumbersome model (teacher) to a compact model (student). Specifically, we compute spatial and channel relation maps separately for the teacher and student models, and then align corresponding relation maps by minimizing their distance. Since the teacher model usually learns more information and collects richer spatial and channel correlations than the student model, transferring these correlations from the teacher to the student can help the student mimic the teacher better in terms of feature distribution, thus improving the segmentation accuracy of the student model. We conduct comprehensive experiments on three segmentation datasets, including two widely adopted benchmarks in the remote sensing field (Vaihingen and Potsdam datasets) and one popular benchmark in general scene (Cityscapes dataset). The experimental results demonstrate that our novel distillation framework can significantly boost the performance of the student network without incurring extra computational overhead.

Keywords: Convolutional Neural Networks, Knowledge Distillation, Semantic Segmentation, Self-attention Mechanism

*Corresponding author

Email addresses: liminglong18@mails.ucas.ac.cn (Minglong Li), shanlianlei18@mails.ucas.ac.cn (Lianlei Shan), wqwang@ucas.ac.cn (Weiqiang Wang), luk@ucas.ac.cn (Ke Lv), luobin@ahu.edu.cn (Bin Luo), sbchen@ahu.edu.cn (Si-Bao Chen)

1. Introduction

Semantic segmentation is a crucial image understanding task that aims to perform per-pixel categorizations for a given image. In recent years, effective methods based on Fully Convolutional Networks (FCNs) [1] have significantly enhanced the accuracy of segmentation. However, the high computational complexity of these models poses a challenge for their efficient deployment on resource-constrained devices, such as edge or IoT devices.

One promising solution to address this challenge is to design novel neural architectures or operators that are more efficient on edge systems without compromising accuracy. For instance, Sandler et al. [2] add linear bottleneck and inverted residual block to improve both accuracy and performance. Zhou et al. [3] combines neural architecture search and NetAdapt to design a more accurate and efficient network architecture. Ma et al.[4] empirically observes four principles for designing efficient CNNs and proposes channel split to improve accuracy and performance. Recently, [5] presents pyramidal fusion, a principled approach for dense recognition based on resolution pyramids, which outperforms all previous semantic segmentation approaches aiming at real-time operation.

In addition to designing computationally efficient architectures, model compression is another popular approach to achieve a trade-off between accuracy and speed. Generally, existing compression methods can be roughly divided into three categories: quantization, pruning, and knowledge distillation. Quantization-based approaches represent the parameters of filter kernels and weighting matrices using fewer bits. Pruning-based methods aim to trim the network by removing redundant connections between neurons of adjacent layers. Knowledge distillation is a way of transferring knowledge from a cumbersome model to a compact model to improve the performance of compact networks.

The notion of knowledge distillation was first proposed in [6]. In the computer vision field, knowledge distillation was initially applied to image classification tasks by using the class probabilities produced from the cumbersome model as soft targets for training the compact model [7] or further transferring the intermediate feature maps [8]. Some recent works have extended knowledge distillation to semantic segmentation tasks. Since the goal of semantic segmentation is to perform per-pixel categorizations for a given image, a straightforward idea to introduce knowledge distillation into semantic segmentation tasks is to align pixel-wise outputs individually. This procedure forces the student model to mimic the teacher model in terms of output probability maps.

However, unlike classification tasks, semantic segmentation involves structured output, where correlations between a certain pixel and other pixels can help accurately classify that pixel. Therefore, correlations between different pixels are crucial for accurate segmentation, especially when the distance between two pixels exceeds the receptive field. The teacher and student models usually capture different long-range contextual information due to their differences in receptive fields. Thus, transferring this information from the teacher to the student helps the student model achieve better segmentation results. Liu et al.[9] present a method to distill structured knowledge from large networks to small

networks, Wang et al. [10] focus on transferring intra-class feature variation from teacher to student, and Li et al.[11] propose a novel dynamic-hierarchical attention distillation network with multimodal synergetic instance selection for land cover classification using missing data modalities. Among these methods,[9] and [10] have made use of spatial relations in feature maps and achieved good results.

Moreover, several works have paid attention to channel relation. [12] models channel and spatial correlation in a single matrix for both teacher and student, then aligns the two matrices using a channel and spatial correlation loss function. Shu et al.[13] apply the softmax normalization to transfer the activation values in each channel into a distribution. They then directly minimize the discrepancy of the channel-wise distribution between the teacher and student network. For a given feature map, contextual relationships not only exist in the spatial dimension but also in the channel dimension. The work [13] ignores the relation between different channels and implement channel distillation separately for each channel. In contrast, our framework considers spatial and channel relation simultaneously. We name our method Dual Relation Distillation (DRD). Unlike [12], we model spatial and channel relation separately and build two relation maps for both teacher and student. Additionally, we use a different method to build the channel relation map.

In summary, we propose a novel Dual Relation Distillation (DRD) framework to transfer both spatial and channel relations in feature maps from the teacher model to the student model. Our proposed method shows better performance compared to previous works in aerial scenes. With a combination of two other useful techniques, our DRD significantly boosts the accuracy of the student model in two aerial benchmarks. We further test the generalization performance of our network in general scenes on the popular Cityscapes dataset. The results show that our DRD achieves better or comparable performance compared to previous works.

The rest of this paper is organized as follows. We briefly review some related works and further clarify the differences with our approach in Section 2. Section 3 introduces the technical details of the proposed dual relation distillation framework. Section 4 presents the experimental results and conducts the analysis. Finally, Section 5 draws conclusions.

2. Related Work

In this section, we briefly review some related works on semantic segmentation, and knowledge distillation.

2.1. Semantic Segmentation

Semantic segmentation is a fundamental topic in computer vision, and the recent rapid development of deep neural networks (DNNs) has had a tremendous impact on its progress. Following the pioneering work [1] that adopts fully convolutional networks for semantic segmentation, many efforts have been made to boost segmentation performance by exploiting multi-scale context. For instance, Chen et al.[14] utilizes dilated convolution to enlarge the receptive field

and preserve the spatial size of the feature map. Chen et al. [15] further develop DeeplabV3+ with an encoder-decoder structure to recover spatial information. PSPNet [16] applies pyramid pooling to aggregate contextual information. Hu et al.[17] present a lightweight and efficient network model LADNet for real-time semantic segmentation tasks. Gao et al. [18] also present a novel lightweight network MSCFNet that uses an asymmetric encoder-decoder architecture and efficient attention modules to achieve a good balance between accuracy, inference speed, and model size for real-time semantic segmentation applications. Zhou et al. [19] presents a network CENet than employs the encoder-decoder architecture to fully explore contextual features through an ensemble of dense deconvolutions.

Recently, attention mechanisms have been used to guide network learning and alleviate inconsistency in segmentation. For example, [20] adopts channel attention to select features, while [21] considers the combination of spatial and channel attention. These state-of-the-art methods aim to boost segmentation performance at the cost of high computational resources.

To address this issue, highly efficient semantic segmentation has been recently studied. ESPNet [22] designs an efficient spatial pyramid module that decomposes the standard convolution into point-wise convolution followed by spatial pyramid to reduce computational cost. In [23], the authors propose ICNet, an image cascade network based on the compressed PSPNet for real-time semantic segmentation. Yu et al.[24] introduce BiSeNet, which contains a spatial path and a context path to raise efficiency.

2.2. Knowledge Distillation

In recent years, knowledge distillation has been extensively researched. Knowledge distillation enables the student model to achieve high accuracy while maintaining efficiency. Several knowledge distillation schemes have been proposed recently. Zagoruyko et al. [8] transfer the attention map of the teacher model to the student model. Yim et al. [25] consider the flow knowledge between layers. [26] introduce correlation congruence for knowledge distillation to transfer not only the instance-level information but also the correlation between instances. Xu et al. [27, 28] apply knowledge distillation based on conditional adversarial networks.

Early works of knowledge distillation have primarily focused on image classification. However, with the growing interest in this topic, knowledge distillation approaches have been introduced into other vision tasks, including semantic segmentation. [29] adapts knowledge distillation with an additional auto-encoder and transfers densely pairwise affinity maps to the student model. [9] proposes structured knowledge distillation (SKD), which transfers pairwise relations and forces the outputs of the student model to mimic the teacher model from a holistic view via adversarial learning.[10] proposes intra-class feature variation distillation (IFVD) to transfer the intra-class feature variation (IFV) of the cumbersome model to the compact model. The self-attention distillation (SAD) is introduced in [30] to explore attention maps derived from high-level features as the distillation target for shallow layers.

For a given feature map, contextual relationships not only exist in the spatial dimension but also in the channel dimension. However, [9] only models the relationship in the spatial dimension and does not utilize the information in the channel dimension. Recently, some works have become concerned about channel correlation. [12] models channel and spatial correlation in a single matrix for both teacher and student, then aligns the two matrices using a channel and spatial correlation loss function. [13] applies the softmax normalization to transfer the activation values in each channel into a distribution, then directly minimizes the discrepancy of the channel-wise distribution between the teacher and student network. However, [13] ignores the relation between different channels and implement channel distillation separately for each channel. In contrast, the proposed Dual Relation Distillation (DRD) framework models spatial and channel relations simultaneously. We build two relation maps for both teacher and student, which is different from [12]. And others also do some meaningful works in segmentation [31, 32, 33, 34, 35, 36, 37, 38, 39, 40, 41, 42, 43, 44, 45, 46, 47, 48, 49, 50, 51, 52, 53, 54, 55, 56, 57, 58, 59, 60, 61].

3. Method

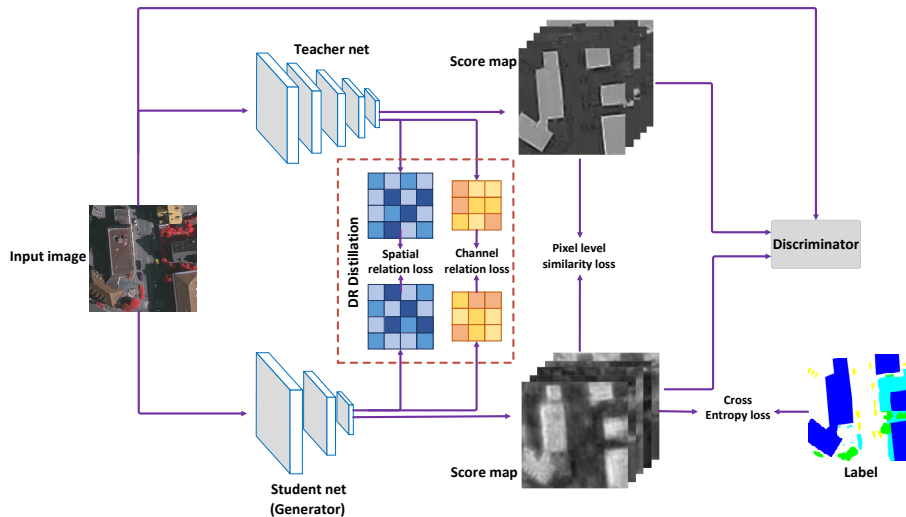


Figure 1: Pipeline of the proposed Dual Relation Distillation (DRD). (Example from Vaihingen dataset, best viewed in color.)

In this section, we present the proposed Dual Relation Distillation (DRD) pipeline. An overview of our method is illustrated in Figure 1. We design the teacher network to have a deeper encoder than the student network. To effectively transfer knowledge from the teacher network to the student network, we

equip our pipeline with four types of loss functions, in addition to the commonly used cross-entropy loss for pixel categorization.

3.1. Dual Relation Alignment in Feature Map

Due to the different sizes of the receptive field in the student and teacher networks, the features corresponding to pixels with the same label may have some differences. Therefore, we propose a spatial relation loss and a channel relation loss to transfer rich information from the teacher feature map to the student feature map.

Given an input feature map $\mathcal{F} \in \mathbb{R}^{C \times H \times W}$, where W and H are the width and height of the feature map, respectively, and C is the number of channels, we first reshape it to matrix $\mathbf{F} \in \mathbb{R}^{C \times N}$, where $N = H \times W$ is the total number of pixels in the feature map. Next, we perform a matrix multiplication $\mathbf{F}^T \mathbf{F}$ between \mathbf{F} and its transpose, \mathbf{F}^T . We then apply a softmax layer to calculate the spatial relation map, $\mathbf{S} \in \mathbb{R}^{N \times N}$,

$$s_{ij} = \frac{\exp(F_j^T F_i)}{\sum_{j=1}^N \exp(F_j^T F_i)} \quad (1)$$

where F_i denotes the feature of pixel i , which corresponds to the i th column of matrix \mathbf{F} , and s_{ij} denotes the normalized affinity of pixel j with respect to pixel i . The larger the value s_{ij} in the relation map \mathbf{S} is, the stronger the relative correlation of pixel j with respect to pixel i is.

To minimize the distance between the spatial relation maps of the teacher network t and the student network s , we utilize the conventional Mean Squared (L2) loss as shown below:

$$L_S = \frac{1}{(N \times N)} \sum_{i=1}^N \sum_{j=1}^N (s_{ij}^s - s_{ij}^t)^2. \quad (2)$$

Spatial relations mainly capture long-range dependencies from the teacher network, which are difficult to learn for small models due to their limited receptive field and abstraction capability. For a given feature map, contextual relationships not only exist in the spatial dimension but also in the channel dimension, especially in high-level features. Intuitively, each channel of the high-level feature map can be regarded as a class-specific response, and different semantic responses are associated with each other. Therefore, we can evaluate a channel relation map $\mathbf{C} = (c_{ij}) \in \mathbb{R}^{C \times C}$, and we propose a channel relation loss similar to the spatial relation loss for training the student network. The loss function is defined as follows:

$$L_C = \frac{1}{(C \times C)} \sum_{i=1}^C \sum_{j=1}^C (c_{ij}^s - c_{ij}^t)^2, \quad (3)$$

where c_{ij} denotes the normalized affinity of channel j with respect to channel i , and the superscripts s and t is used to distinguish between the student and

teacher networks. The normalized affinity c_{ij} is computed by

$$c_{ij} = \frac{\exp\left(\hat{F}_j \hat{F}_i^T\right)}{\sum_{j=1}^C \exp\left(\hat{F}_j \hat{F}_i^T\right)}, \quad (4)$$

where \hat{F}_i denotes the features of all pixels in channel i , which corresponds to the i th row of matrix \mathbf{F} , and c_{ij} denotes the normalized affinity of channel j with respect to channel i . The larger the value c_{ij} in the relation map \mathbf{C} is, the stronger the relative correlation of channel j with respect to channel i is.

Considering that the student model should not only mimic the feature distribution, but also the output score map of the teacher model, we also include the loss of original knowledge distillation and adversarial learning in our pipeline.

3.2. Pixel-Level Similarity Alignment in Score Map

We view the segmentation problem as a collection of individual pixel labeling tasks and utilize knowledge distillation to align the class probabilities of each pixel generated by the compact network. Our approach is straightforward: we use the class probabilities generated by the cumbersome model as soft targets to train the compact network.

The loss function is defined as follows,

$$L_P = \frac{1}{N} \sum_{i=1}^N \text{KL}(\mathbf{q}_i^t \parallel \mathbf{q}_i^s) \quad (5)$$

where \mathbf{q}_i^s represents the class probabilities of the i th pixel produced from the compact network s , and \mathbf{q}_i^t represents the class probabilities of the i th pixel produced from the cumbersome network t . Both \mathbf{q}_i^s and \mathbf{q}_i^t are vectors of size $1 \times 1 \times c$, where c denotes the number of classes in the segmentation task. N denotes the total number of pixels in the feature map. $\text{KL}(\cdot)$ denotes the Kullback-Leibler divergence between two probabilities, which is calculated as follows:

$$\text{KL}(\mathbf{q}_i^t \parallel \mathbf{q}_i^s) = \sum_{i=1}^N \sum_{j=1}^c \mathbf{q}_{ij}^t \cdot \log \frac{\mathbf{q}_{ij}^t}{\mathbf{q}_{ij}^s}, \quad (6)$$

where \mathbf{q}_{ij}^t and \mathbf{q}_{ij}^s denote the j th entry of class probability vectors \mathbf{q}_i^s and \mathbf{q}_i^t , respectively.

3.3. Global Similarity Alignment through Adversarial Learning

We employ an adversarial training approach to ensure that the holistic embeddings of the segmentation maps generated by the compact segmentation network are indistinguishable from those produced by the cumbersome segmentation network. This technique, known as adversarial learning for knowledge distillation, was first introduced in [27]. A similar approach, called holistic distillation, was proposed in [9] for semantic segmentation. We also incorporate

adversarial learning in the output space. Specifically, we first train a discriminator to differentiate between inputs from the teacher model and the student model by evaluating the similarity between the raw image and the segmentation map. The segmentation network is then trained to deceive the discriminator. The loss functions for training the discriminator (L_d) and the adversarial item (L_{adv}) can be formulated as follows:

$$L_d = \mathbb{E}_{z_s \sim p_s(z_s)} [D(z_s | I)] - \mathbb{E}_{z_t \sim p_t(z_t)} [D(z_t | I)], \quad (7)$$

$$L_{Adv} = \mathbb{E}_{z_s \sim p_s(z_s)} [D(z_s | I)]. \quad (8)$$

For our proposed dual relation distillation (DRD), the total loss as the training objective function is composed of a conventional cross-entropy loss L_{CE} for semantic segmentation and three loss items for knowledge distillation:

$$L_{total} = L_{CE} + \lambda_1 L_P - \lambda_2 L_{Adv} + \lambda_3 (L_S + L_C), \quad (9)$$

where $\lambda_1, \lambda_2, \lambda_3$ are set to 10, 0.1 and 25, respectively.

4. Experiments

4.1. Datasets

4.1.1. Vaihingen Dataset

The Vaihingen dataset comprises 33 aerial images covering a 1.38 km² area of the city of Vaihingen, with a spatial resolution of 9 cm. Each image has an average size of 2494 × 2064 pixels and three bands corresponding to near-infrared (NIR), red (R), and green (G) wavelengths. Additionally, DSMs, which indicate the height of all object surfaces in an image, are provided as complementary data. Out of the 33 images, 16 are manually annotated with pixel-wise labels, and each pixel is classified into one of six land cover classes: buildings, cars, low vegetation, impervious surfaces, trees, and clutter/background. Clutter/background is not considered when counting loss. Following the setup in [62], we use 11 images for training, and the remaining five images (image IDs: 11, 15, 28, 30, 34) are used to test our model.

4.1.2. Potsdam Dataset

The Potsdam dataset comprises 38 high-resolution aerial images covering an area of 3.42 km², with each image captured in four channels (NIR, R, G, and blue (B)). All images are of size 6000 × 6000 pixels and are annotated with pixel-level labels of six classes, similar to the Vaihingen dataset. The spatial resolution is 5 cm, and coregistered DSMs are also available. For training and evaluating networks, we use 17 images for training and build the test set with the remaining images (image IDs: 02_11, 02_12, 04_10, 05_11, 06_07, 07_08, 07_10), following the setup in [62].

4.1.3. Cityscapes Dataset

The Cityscapes dataset is designed for urban scene understanding and consists of 30 classes, with only 19 classes used for evaluation. The dataset includes 5,000 high-quality pixel-level finely annotated images and 20,000 coarsely annotated images. The finely annotated 5,000 images are divided into 2,975/500/1,525 images for training, validation, and testing. In our experiments, we only use the finely annotated parts of the dataset in our experiments.

4.2. Evaluation Metric

To evaluate the performance of our DRD, we introduce various evaluation metrics. Firstly, we calculate F_1 score for each category with the following formula:

$$F_1 = (1 + \beta^2) \cdot \frac{\text{precision} \cdot \text{recall}}{\beta^2 \cdot \text{precision} + \text{recall}}, \quad \beta = 1. \quad (10)$$

Furthermore, we compute the mean F_1 score by averaging all F_1 scores to assess models impartially. Notably, a higher F_1 score indicates a better result.

In addition, we also calculate the Overall Accuracy (OA) and mean Intersection over Union (mIOU) of all categories to provide a detailed and comprehensive comparison with different methods. The Overall Accuracy is calculated by counting the proportion of correctly classified pixels to all pixels. The concrete computation is defined as follows,

$$\text{OA} = \frac{\sum_{i=1}^M p_{ii}}{\sum_{i=1}^M \sum_{j=1}^M p_{ij}} \quad (11)$$

where p_{ij} denotes the number of pixels that actually belong to category i and are predicted to be category j , and M is the total number of all the categories.

For a specific category, the intersection and union ratio can be calculated using the following formula:

$$\text{IoU} = \frac{|y \cap \hat{y}|}{|y \cup \hat{y}|}, \quad (12)$$

where \hat{y} and y represent the region corresponding to the category in the predicted segmentation result and the ground truth, respectively. The accuracy of the model’s prediction is measured by the overlap ratio of the two regions. The mean intersection over union ratio is the unweighted average of the intersection over union ratio of each category.

Additionally, we also calculate the model size and complexity. The model size is represented by the number of network parameters, while the model complexity is evaluated by the sum of floating point operations (FLOPs) in one forward pass on a fixed resolution of 512×1024 using the PyTorch implementation ¹

¹https://github.com/warmspringwinds/pytorch-segmentation-detection/blob/master/pytorch_segmentation_detection/utils/flops_benchmark.py

4.3. Implementation details

4.3.1. Network architectures

To ensure a fair comparison, we conduct the experiments using the same cumbersome and compact networks as [9] and [10]. Specifically, we use the segmentation architecture PSPNet [16] with ResNet101 [63] backbone as the teacher model for all experiments. The student model also utilizes PSPNet as the segmentation architecture, but with different backbone networks. We conduct the experiments on ResNet18 [63] and ResNet18 (0.5), which is the width-halved version of ResNet18, as the backbone for the student model.

4.3.2. Training details

For aerial benchmark, since the resolution of remote sensing image is too high, it cannot be directly used for model training and testing. When training with the subsampled high-resolution remote sensing images, the segmentation performance is poor thanks to the loss of too much detailed information. Therefore, we choose to crop the high-resolution remote sensing image into small slices for training and testing. We choose image crop size as 645×645 for Vaihingen dataset and 600×600 for Potsdam dataset. As for Cityscapes dataset we do not crop the initial images. The implementation is based on the PyTorch platform. All our distillation experiments are carried out on a workstation equipped with a single NVIDIA RTX 3090 GPU card of 24 GB memory.

4.4. Ablation Study

Table 1: Ablation study on Vaihingen dataset. ImN means initial from the ImageNet-pre-trained weights

Method	L_P	L_{Adv}	L_S	L_C	mean F_1 (%)	mIoU(%)	OA(%)
Teacher(ResNet101)					86.07	75.99	86.67
ResNet18					79.15	66.53	83.09
ResNet18	✓				79.88	67.47	83.73
ResNet18	✓	✓			80.16	67.79	83.79
ResNet18	✓	✓	✓		80.40	68.18	84.18
ResNet18	✓	✓	✓	✓	80.83	68.62	83.94
ResNet18(IMN)					81.13	68.94	83.74
ResNet18(IMN)	✓				82.81	71.27	84.89
ResNet18(IMN)	✓	✓			83.12	71.69	85.27
ResNet18(IMN)	✓	✓	✓		83.59	72.33	85.26
ResNet18(IMN)	✓	✓	✓	✓	84.03	72.95	85.46

In this section, we conduct ablation studies on the Vaihingen dataset to demonstrate the effectiveness of our technical contributions in Section 3. Our proposed DRD includes four loss items for knowledge distillation: L_P , L_{Adv} , L_S , and L_C . Therefore, we study their contributions individually. We first train the teacher model PSPNet with ResNet101 backbone and then perform

knowledge distillation on the student model with ResNet18 backbone. Table 1 presents the results of different settings for the student network. As shown, knowledge distillation improves the performance of the student network, and distilling the relation information in the feature map helps the student learn better. With the four distillation terms, the improvements for ResNet18 and ResNet18 with ImageNet-pretrained weights are 1.68%, 2.90% in mean F_1 and 2.10%, 4.01% in mIoU, respectively. Additionally, each distillation scheme leads to a higher mean F_1 score and mIoU score, indicating that the four distillation schemes make complementary contributions to better train the compact network. After distillation, the best mIoU for ResNet18(IMN) reaches 72.95% on the test set, and the gap between the student and teacher is reduced from 7.05% to 3.04% when both are initialized from ImageNet-pretrained weights. These results demonstrate the effectiveness of the proposed DRD.

4.5. Comparison with Existing Works

Table 2: Experimental Results on the Vaihingen Dataset.

Method	Imp. surf.	Build.	Low veg.	Tree	Car	mean F_1	mIoU	OA	Params(M)	FLOPs(G)
FCN-dCRF ([64])	88.80	92.99	76.58	86.78	71.75	83.38	72.28	86.65	-	-
FCN ([1])	88.67	92.83	76.32	86.67	74.21	83.74	72.69	86.51	134.5	333.9
SCNN ([65])	88.21	91.80	77.17	87.23	78.60	84.40	73.73	86.43	-	-
Dilated FCN ([14])	90.19	94.49	77.69	87.24	76.77	85.28	-	87.70	262.1	457.8
FCN-FR ([66])	91.69	95.24	79.44	88.12	78.42	86.58	-	88.92	-	-
S-RA-FCN [62]	91.47	94.97	80.63	88.57	87.05	88.54	79.76	89.23	-	-
Teacher: PSPNet(ResNet101)	89.38	94.19	76.80	85.40	84.57	86.07	75.99	86.67	70.43	574.9
ResNet18(0.5)	85.15	90.46	72.24	82.57	61.48	78.38	65.59	82.69	3.27	31.53
ResNet18(0.5) + IFVD* [10]	84.70	90.37	72.09	82.73	65.31	79.04	66.26	82.59	3.27	31.53
ResNet18(0.5) + SKD* [9]	86.60	91.11	73.65	83.33	67.93	80.52	68.24	83.82	3.27	31.53
ResNet18(0.5) + DRD	86.69	90.96	73.73	83.42	71.77	81.31	69.17	83.91	3.27	31.53
ResNet18	86.30	91.26	73.19	83.48	71.39	81.13	68.94	83.74	13.07	125.8
ResNet18 + IFVD* [10]	87.04	92.46	74.06	84.08	75.91	82.71	71.11	84.58	13.07	125.8
ResNet18 + SKD* [9]	87.84	92.62	75.44	84.51	77.54	83.59	72.33	85.26	13.07	125.8
ResNet18 + DRD	87.99	92.64	75.28	84.90	79.36	84.03	72.95	85.46	13.07	125.8

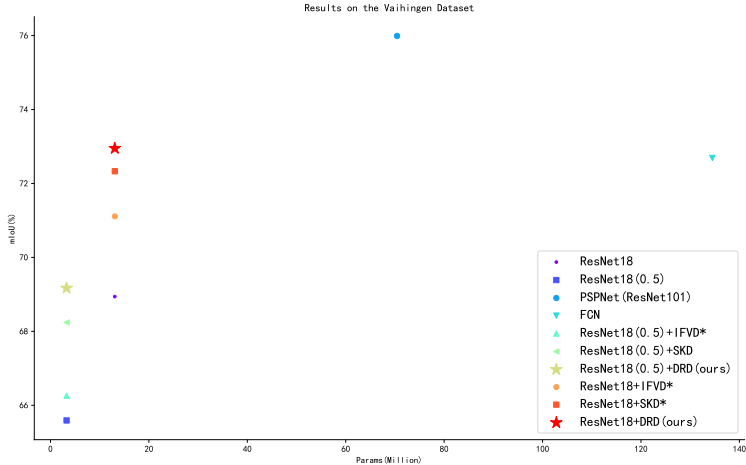


Figure 2: Performance (mIoU (%)) vs. models sizes of some methods in Table 2 on Vaihingen Dataset.

We then evaluate our proposed DRD on the Vaihingen dataset and compare it with existing works. The quantitative results are listed in Table 2, which includes the F_1 score of each class, overall segmentation accuracy (mean F_1 , mIoU, OA), model size, and model complexity. Since the methods of [9] and [10] do not provide experimental results in aerial datasets, we evaluate [9] and [10] with their given codes in the Vaihingen dataset, and the results are denoted by *.

Our distillation approach has shown significant improvements in three evaluation metrics for two compact networks: ResNet18 (0.5) and ResNet18. Specifically, our DRD improves the student model built on ResNet18 without distillation by 2.90%, 4.01%, and 1.72% in mean F_1 , mIoU, and Overall Accuracy, respectively, with a gain of 0.44%, 0.62%, and 0.20% compared to the previous method [9]. We also applied the proposed distillation scheme on another backbone, ResNet18 (0.5), a width-halved version of the original ResNet18 without ImageNet-pre-trained weights. The proposed DRD improves the student model based on ResNet18 (0.5) backbone by 2.93%, 3.58%, and 1.22% in mean F_1 , mIoU, and Overall Accuracy, respectively, with a gain of 0.79%, 0.93%, and 0.09% compared to [9]. These results demonstrate the effectiveness of the proposed DRD method. In order to more clearly demonstrate the performance and model size correlation between the pre and post distillation models, as well as the compact and cumbersome models, we have visually summarized some methods in Table 2 in Figure 2

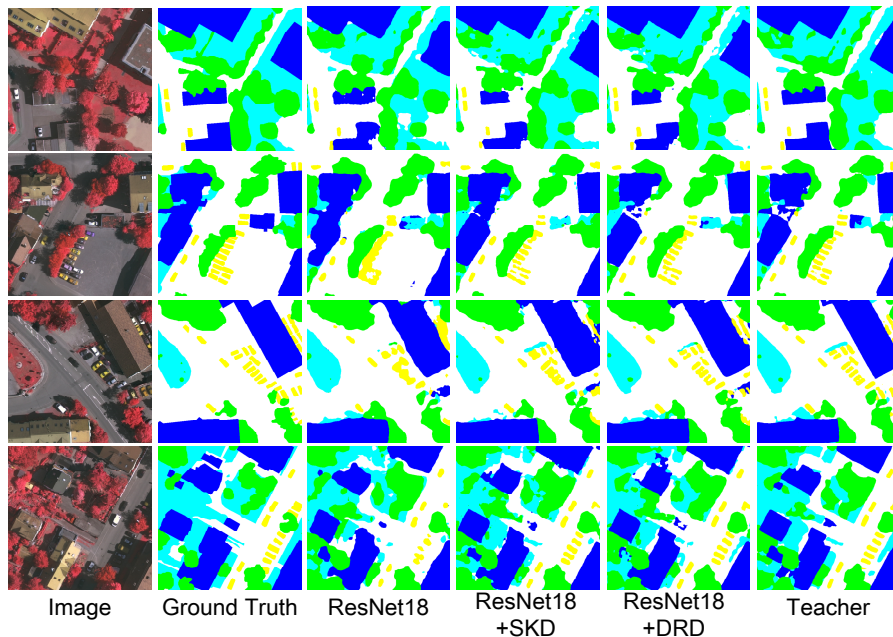


Figure 3: Examples of segmentation results on the Vaihingen dataset. Legend—white: impervious surfaces, blue: buildings, cyan: low vegetation, green: trees, yellow: cars, red: clutter/background. (Best viewed in color.)

Figure 3 shows a few examples of qualitative results on the Vaihingen dataset. By comparing column 3 and column 5, we can clearly see that after distillation using our DRD framework, the student network generates more accurate segmentation results compared to no extra guidance from the teacher network, especially for the previous low-accuracy class such as cars. By comparing column 4 and column 5, we can see that our DRD leads to better results compared to [9]. If we compare the last column with column 3 and column 5, we can conclude that the gap between the student model and teacher model is reduced.

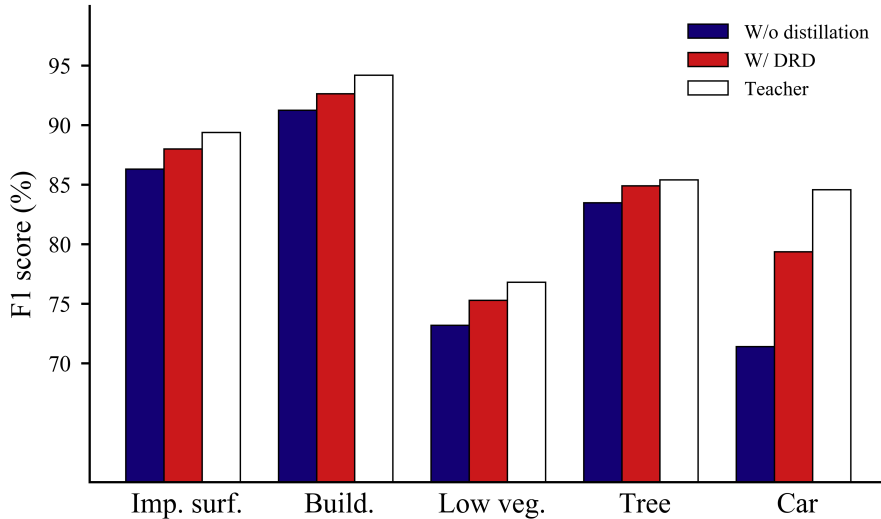


Figure 4: Effectiveness of our DRD on the Vaihingen dataset with ResNet 18.

Figure 4 shows the F_1 score improvements for each category in the student network using ResNet(18) backbone after distillation. As can be seen, our distillation method improves all categories, especially for categories with low accuracy, and reduces the gap between the teacher model and student model after distillation.

4.6. Results on the Potsdam Dataset

Table 3: Experimental Results on the Potsdam Dataset.

Method	Imp. surf.	Build.	Low veg.	Tree	Car	mean F_1	mIoU	OA	Params(M)	FLOPs(G)
Dilated FCN [14]	86.52	90.78	83.01	78.41	90.42	85.83	-	84.14	262.1	457.8
SCNN [65]	88.37	92.32	83.68	80.94	91.17	87.30	77.72	85.57	-	-
FCN [1]	88.61	93.29	83.29	79.83	93.02	87.61	78.34	85.59	134.5	333.9
FCN-dCRF [64]	88.62	93.29	83.29	79.83	93.03	87.61	78.35	85.60	-	-
FCN-FR [66]	89.31	94.37	84.83	81.10	93.56	88.63	-	87.02	-	-
S-RA-FCN [62]	91.33	94.70	86.81	83.47	94.52	90.17	82.38	88.59	-	-
Teacher: PSPNet(ResNet101)	90.91	94.26	86.53	82.06	91.41	89.04	80.50	88.62	70.43	574.9
ResNet18(0.5)	86.50	90.12	82.15	73.93	85.18	83.58	72.16	83.56	3.27	31.53
ResNet18(0.5) + SKD* [9]	88.70	92.71	84.16	79.31	88.52	86.68	76.78	86.38	3.27	31.53
ResNet18(0.5) + IFVD* [10]	88.94	92.78	84.22	78.27	89.44	86.73	76.91	86.28	3.27	31.53
ResNet18(0.5) + DRD	89.29	92.89	84.83	79.85	89.68	87.31	77.76	86.92	3.27	31.53
ResNet18	88.46	92.10	83.48	77.33	88.58	85.99	75.77	85.63	13.07	125.8
ResNet18 + SKD* [9]	90.00	92.93	85.41	79.50	90.14	87.60	78.24	87.30	13.07	125.8
ResNet18 + IFVD* [10]	89.66	93.24	84.99	80.65	90.07	87.72	78.40	87.23	13.07	125.8
ResNet18 + DRD	90.10	93.33	85.72	81.05	90.54	88.15	79.07	87.76	13.07	125.8

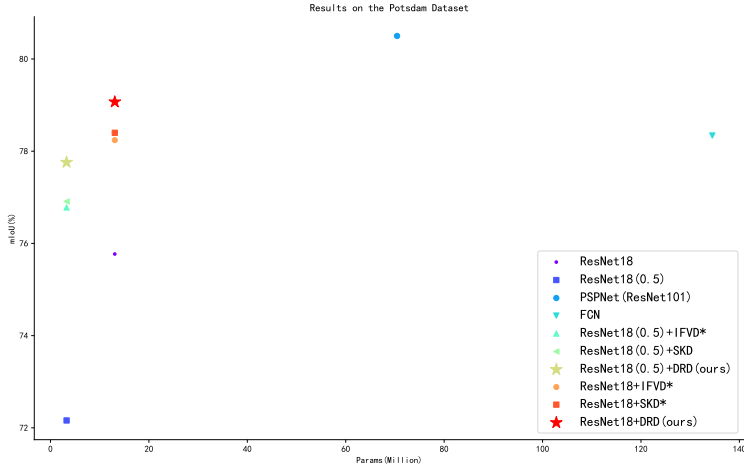


Figure 5: Performance (mIoU (%)) vs. models sizes of some methods in Table 3 on Potsdam Dataset.

To further validate the effectiveness of our network, we conduct experiments on the Potsdam dataset, and the numerical results are shown in Table 3. * denotes the results we reproduce using the released code of [9] and [10]. As can be seen, after distillation, our DRD improves the student model built on ResNet18 without distillation by 2.16%, 3.30%, and 2.13% in mean F_1 , mIoU, and Overall Accuracy, respectively, with a gain of 0.55%, 0.83%, and 0.46% compared to the previous method [9]. We also applied the proposed distillation scheme on ResNet18 (0.5), a width-halved version of the original ResNet18 without ImageNet-pre-trained weights. Our proposed method improves the ResNet18 (0.5) model by 3.73%, 5.60%, and 3.36% in mean F_1 , mIoU, and Overall Accuracy, respectively, with a gain of 0.63%, 0.98%, and 0.54% compared to [9]. These results demonstrate the effectiveness of the proposed DRD. After distillation, the gap between the teacher model and student model in the Potsdam dataset is less than the result in the Vaihingen dataset, which is probably due to the availability of more training data. To more clearly demonstrate the performance and model size correlation between the pre and post distillation models, as well as the compact and cumbersome models, we have visually summarized some methods in Table 3 in Figure 5

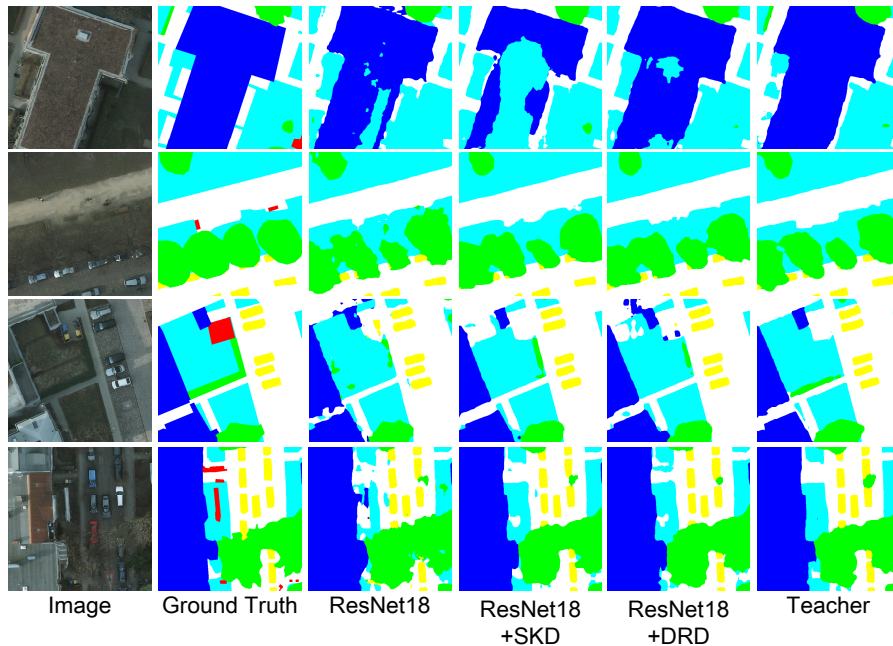


Figure 6: Examples of segmentation results on the Potsdam dataset. Legend—white: impervious surfaces, blue: buildings, cyan: low vegetation, green: trees, yellow: cars, red: clutter/background. (Best viewed in color.)

Figure 6 shows a few examples of qualitative results on the Potsdam dataset. By comparing column 4 and column 5, we can see that our DRD leads to better results compared to [9]. By comparing column 3 and column 5, we can see that after distillation using our DRD framework, the student network generates more accurate segmentation results compared to no extra guidance from the teacher network, especially for the previous low-accuracy class such as trees. If we compare the last column with column 3 and column 5, we can conclude that the gap between the student model and teacher model is reduced after distillation.

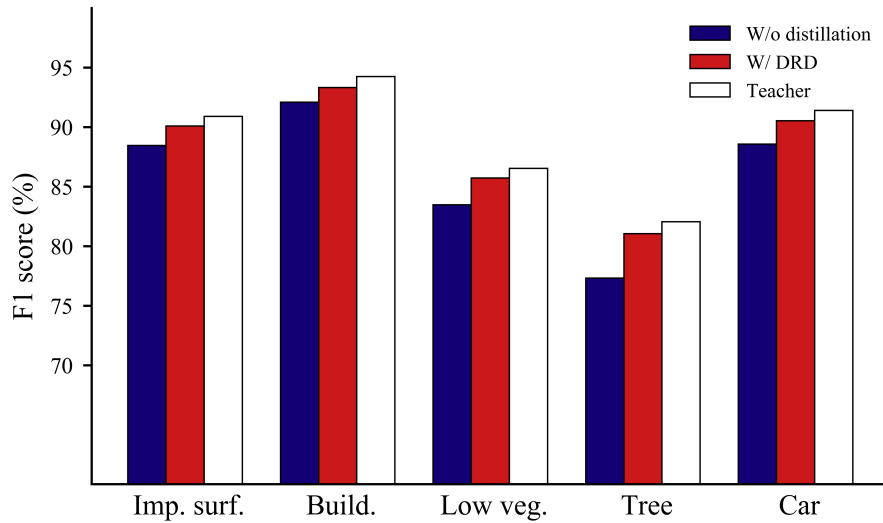


Figure 7: Effectiveness of our DRD on the Potsdam dataset with ResNet 18.

Figure 7 shows the F_1 score improvements for each category in the student network using ResNet(18) backbone after distillation. As can be seen, our distillation method improves all categories, especially for categories with low accuracy, and reduces the gap between the teacher model and student model after distillation.

4.7. Results on the Cityscapes Dataset

Table 4: Experimental Results on the Cityscapes Dataset.

Method	val mIoU(%)	test mIoU(%)	Params(M)	FLOPs(G)
ENet [67]	-	58.3	0.3580	3.612
ESPNet [22]	-	60.3	0.3635	4.422
ERFNet [68]	-	68.0	2.067	25.60
FCN [1]	-	65.3	134.5	333.9
RefineNet [69]	-	73.6	118.1	525.7
PSPNet [70]	-	78.4	70.43	574.9
Teacher: PSPNet(ResNet101)	78.56	76.78	70.43	574.9
ResNet18(0.5)	55.40	54.10	3.27	31.53
ResNet18(0.5) + SKD [9]	61.60	60.50	3.27	31.53
ResNet18(0.5) + IFVD [10]	63.35	63.68	3.27	31.53
ResNet18(0.5) + DRD	62.92	62.87	3.27	31.53
ResNet18	69.10	67.60	13.07	125.8
ResNet18 + SKD [9]	72.70	71.40	13.07	125.8
ResNet18 + IFVD [10]	74.54	72.74	13.07	125.8
ResNet18 + DRD	73.47	72.75	13.07	125.8

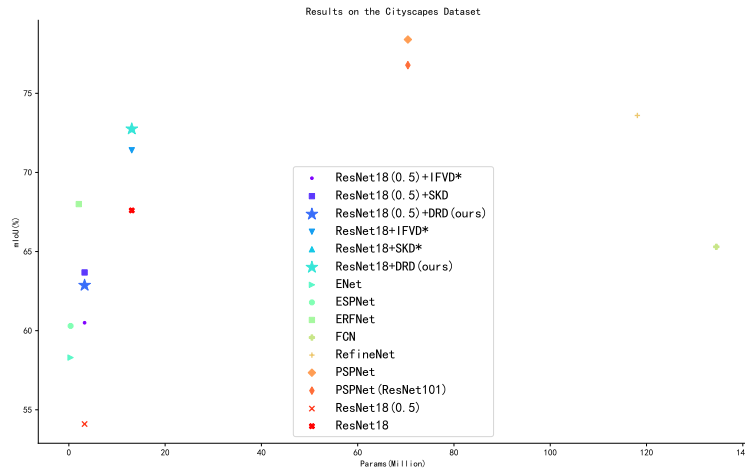


Figure 8: Performance (mIoU (%)) vs. models sizes of some methods in Table 4 on Cityscapes Dataset.

To test the generalization performance of our network, we conduct further experiments on the Cityscapes dataset, a popular benchmark for general scene segmentation. The numerical results are shown in Table 4, which includes the

total segmentation accuracy measured by mIoU, model size, and model complexity.

Our distillation approach improves the segmentation results on both the validation set and test set for two compact networks: ResNet18 (0.5) and ResNet18. Specifically, our DRD improves the student model using the ResNet18 backbone by 4.37% on the validation set and 4.49% on the test set after distillation. When we set the backbone as ResNet18 (0.5), a width-halved version of the original ResNet18 that is not pre-trained on ImageNet, our DRD leads to an improvement of 7.52% on the validation set and 8.77% on the test set. Compared to previous work, our DRD generates better or comparable results. To clearly demonstrate the performance and model size correlation between the pre and post distillation models, as well as the compact and cumbersome models, we have visually summarized some methods in Table 4 in Figure 8

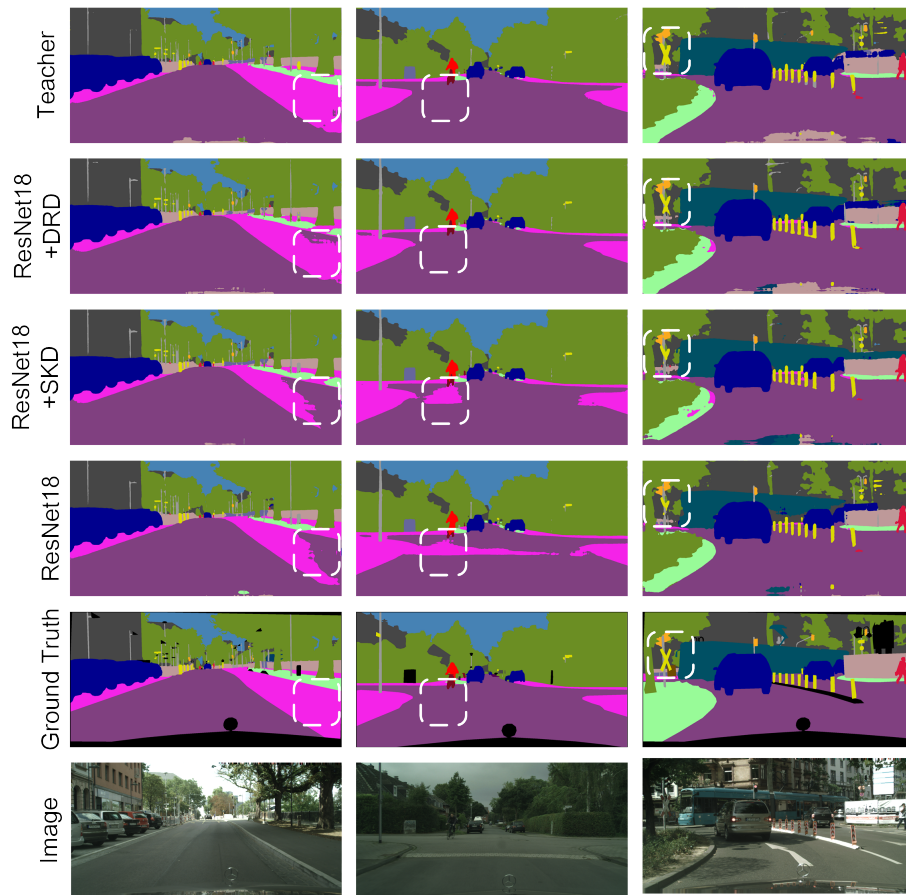


Figure 9: Examples of segmentation results on the Cityscapes dataset.(Best viewed in color.)

Figure 9 shows a few examples of qualitative results on the Cityscapes dataset. In the figure, we use dashed rectangular boxes to highlight the areas that require special attention. The segmentation results in these areas can reflect the differences in segmentation results among different methods. If we compare the top row with row 1, row 2, row 3 and row 4, we can conclude that the gap between the student model and teacher model is reduced after distillation, and the student network generates more accurate segmentation results compared to no extra guidance from the teacher network. By comparing row 2 and row 3, we can see that our DRD leads to better segmentation results compared to [9].

5. Conclusion

In this paper, we have investigated knowledge distillation for training compact semantic segmentation networks with the assistance of cumbersome networks. We have proposed a novel dual relation distillation framework to transfer rich correlation information in feature maps from the teacher network to the student network. These correlations help the student mimic the teacher better in terms of feature distribution, thereby improving the segmentation accuracy of the student model. The comprehensive experimental results have shown that the proposed distillation framework has achieved better or comparable performance compared to previous state-of-the-art methods on three benchmark datasets, including aerial scenes and general scenes. We believe that our work can benefit others in the field by providing a new approach to training compact semantic segmentation networks with high accuracy. In the future, we aim to explore the use of other types of networks, such as attention-based networks, to improve the performance of our method.

Conflict of Interest Statement

We declare that we have no financial or personal relationships with other people or organizations that could inappropriately influence (bias) this work.

Acknowledgment

This work is supported by NSFC Key Projects of International (Regional) Cooperation and Exchanges under Grant 61860206004, and NSFC projects under Grant 61976201.

References

- [1] J. Long, E. Shelhamer, T. Darrell, Fully convolutional networks for semantic segmentation, *IEEE Transactions on Pattern Analysis and Machine Intelligence* 39 (4) (2014) 640–651.

- [2] M. Sandler, A. Howard, M. Zhu, A. Zhmoginov, L.-C. Chen, Mobilenetv2: Inverted residuals and linear bottlenecks, in: Proceedings of the IEEE Conference on Computer Vision and Pattern Recognition (CVPR), 2018.
- [3] D. Zhou, Q. Hou, Y. Chen, J. Feng, S. Yan, Rethinking bottleneck structure for efficient mobile network design, in: A. Vedaldi, H. Bischof, T. Brox, J.-M. Frahm (Eds.), Computer Vision – ECCV 2020, Springer International Publishing, Cham, 2020, pp. 680–697.
- [4] N. Ma, X. Zhang, H.-T. Zheng, J. Sun, Shufflenet v2: Practical guidelines for efficient cnn architecture design, in: The European Conference on Computer Vision (ECCV), 2018.
- [5] M. Oršić, S. Šegvić, Efficient semantic segmentation with pyramidal fusion, Pattern Recognition 110 (2021) 107611.
- [6] C. Bucila, R. Caruana, A. Niculescu-Mizil, Model compression, in: ACM SIGKDD International Conference on Knowledge Discovery and Data Mining(KDD’06), 2006.
- [7] L. J. Ba, R. Caruana, Do deep nets really need to be deep?, in: Proceedings of the 27th International Conference on Neural Information Processing Systems - Volume 2, NIPS’14, MIT Press, Cambridge, MA, USA, 2014, p. 2654–2662.
- [8] S. Zagoruyko, N. Komodakis, Paying more attention to attention: Improving the performance of convolutional neural networks via attention transfer, in: ICLR, 2017.
- [9] Y. Liu, K. Chen, C. Liu, Z. Qin, Z. Luo, J. Wang, Structured knowledge distillation for semantic segmentation, in: Proceedings of the IEEE/CVF Conference on Computer Vision and Pattern Recognition (CVPR), 2019.
- [10] Y. Wang, W. Zhou, T. Jiang, X. Bai, Y. Xu, Intra-class feature variation distillation for semantic segmentation, in: Computer Vision–ECCV 2020: 16th European Conference, Glasgow, UK, August 23–28, 2020, Proceedings, Part VII 16, Springer, 2020, pp. 346–362.
- [11] X. Li, L. Lei, Y. Sun, G. Kuang, Dynamic-hierarchical attention distillation with synergetic instance selection for land cover classification using missing heterogeneity images, IEEE Transactions on Geoscience and Remote Sensing 60 (2021) 1–16.
- [12] S. Park, Y. S. Heo, Knowledge distillation for semantic segmentation using channel and spatial correlations and adaptive cross entropy, Sensors 20 (16) (2020) 4616.
- [13] C. Shu, Y. Liu, J. Gao, Z. Yan, C. Shen, Channel-wise knowledge distillation for dense prediction, in: Proceedings of the IEEE/CVF International Conference on Computer Vision (ICCV), 2021, pp. 5311–5320.

- [14] L. C. Chen, G. Papandreou, I. Kokkinos, K. Murphy, A. L. Yuille, Deeplab: Semantic image segmentation with deep convolutional nets, atrous convolution, and fully connected crfs, *IEEE Transactions on Pattern Analysis and Machine Intelligence* 40 (4) (2018) 834.
- [15] L.-C. Chen, Y. Zhu, G. Papandreou, F. Schroff, H. Adam, Encoder-decoder with atrous separable convolution for semantic image segmentation, in: *The European Conference on Computer Vision (ECCV)*, 2018.
- [16] H. Zhao, J. Shi, X. Qi, X. Wang, J. Jia, Pyramid scene parsing network, in: *CVPR*, 2017.
- [17] X. Hu, Y. Gong, Lightweight asymmetric dilation network for real-time semantic segmentation, *IEEE Access* 9 (2021) 55630–55643.
- [18] G. Gao, G. Xu, Y. Yu, J. Xie, J. Yang, D. Yue, Mscfnet: a lightweight network with multi-scale context fusion for real-time semantic segmentation, *IEEE Transactions on Intelligent Transportation Systems* 23 (12) (2021) 25489–25499.
- [19] Q. Zhou, X. Wu, S. Zhang, B. Kang, Z. Ge, L. J. Latecki, Contextual ensemble network for semantic segmentation, *Pattern Recognition* 122 (2022) 108290.
- [20] C. Yu, J. Wang, C. Peng, C. Gao, G. Yu, N. Sang, Learning a discriminative feature network for semantic segmentation, in: *Proceedings of the IEEE Conference on Computer Vision and Pattern Recognition (CVPR)*, 2018.
- [21] J. Fu, J. Liu, H. Tian, Y. Li, Y. Bao, Z. Fang, H. Lu, Dual attention network for scene segmentation, in: *The IEEE Conference on Computer Vision and Pattern Recognition (CVPR)*, 2019.
- [22] S. Mehta, M. Rastegari, A. Caspi, L. Shapiro, H. Hajishirzi, Espnet: Efficient spatial pyramid of dilated convolutions for semantic segmentation, in: *The European Conference on Computer Vision (ECCV)*, 2018.
- [23] H. Zhao, X. Qi, X. Shen, J. Shi, J. Jia, Icnnet for real-time semantic segmentation on high-resolution images, in: *The European Conference on Computer Vision (ECCV)*, 2018.
- [24] C. Yu, J. Wang, C. Peng, C. Gao, G. Yu, N. Sang, Bisenet: Bilateral segmentation network for real-time semantic segmentation, in: *The European Conference on Computer Vision (ECCV)*, 2018.
- [25] J. Yim, D. Joo, J. Bae, J. Kim, A gift from knowledge distillation: Fast optimization, network minimization and transfer learning, in: *Proceedings of the IEEE conference on computer vision and pattern recognition*, 2017, pp. 4133–4141.

- [26] B. Peng, X. Jin, J. Liu, D. Li, Y. Wu, Y. Liu, S. Zhou, Z. Zhang, Correlation congruence for knowledge distillation, in: Proceedings of the IEEE/CVF International Conference on Computer Vision (ICCV), 2019.
- [27] Z. Xu, Y. Hsu, J. Huang, Training student networks for acceleration with conditional adversarial networks, in: British Machine Vision Conference (BMVC), 2018.
- [28] B. Sambaturu, A. Gupta, C. Jawahar, C. Arora, Scribblenet: Efficient interactive annotation of urban city scenes for semantic segmentation, Pattern Recognition 133 (2023) 109011.
- [29] T. He, C. Shen, Z. Tian, D. Gong, C. Sun, Y. Yan, Knowledge adaptation for efficient semantic segmentation, in: Proceedings of the IEEE/CVF Conference on Computer Vision and Pattern Recognition (CVPR), 2019.
- [30] Y. Hou, Z. Ma, C. Liu, C. C. Loy, Learning lightweight lane detection cnns by self attention distillation, in: Proceedings of the IEEE/CVF International Conference on Computer Vision (ICCV), 2019.
- [31] L. Shan, W. Wang, Densenet-based land cover classification network with deep fusion, IEEE Geoscience and Remote Sensing Letters 19 (2021) 1–5.
- [32] L. Shan, M. Li, X. Li, Y. Bai, K. Lv, B. Luo, S.-B. Chen, W. Wang, Uhrsnet: A semantic segmentation network specifically for ultra-high-resolution images, in: 2020 25th International Conference on Pattern Recognition (ICPR), IEEE, 2021, pp. 1460–1466.
- [33] L. Shan, W. Wang, K. Lv, B. Luo, Class-incremental learning for semantic segmentation in aerial imagery via distillation in all aspects, IEEE Transactions on Geoscience and Remote Sensing 60 (2021) 1–12.
- [34] L. Shan, X. Li, W. Wang, Decouple the high-frequency and low-frequency information of images for semantic segmentation, in: ICASSP 2021-2021 IEEE International Conference on Acoustics, Speech and Signal Processing (ICASSP), IEEE, 2021, pp. 1805–1809.
- [35] L. Shan, W. Wang, Mbnet: A multi-resolution branch network for semantic segmentation of ultra-high resolution images, in: ICASSP 2022-2022 IEEE International Conference on Acoustics, Speech and Signal Processing (ICASSP), IEEE, 2022, pp. 2589–2593.
- [36] L. Shan, W. Wang, K. Lv, B. Luo, Class-incremental semantic segmentation of aerial images via pixel-level feature generation and task-wise distillation, IEEE Transactions on Geoscience and Remote Sensing 60 (2022) 1–17.
- [37] M. Li, L. Shan, X. Li, Y. Bai, D. Zhou, W. Wang, K. Lv, B. Luo, S.-B. Chen, Global-local attention network for semantic segmentation in aerial images, in: 2020 25th International Conference on Pattern Recognition (ICPR), IEEE, 2021, pp. 5704–5711.

- [38] W. Wu, Y. Zhao, Z. Li, L. Shan, H. Zhou, M. Z. Shou, Continual learning for image segmentation with dynamic query, *IEEE Transactions on Circuits and Systems for Video Technology* 34 (6) (2023) 4874–4886.
- [39] L. Shan, W. Zhou, G. Zhao, Incremental few shot semantic segmentation via class-agnostic mask proposal and language-driven classifier, in: *Proceedings of the 31st ACM International Conference on Multimedia*, 2023, pp. 8561–8570.
- [40] L. S. W. Z. G. Zhao, Boosting general trimap-free matting in the real-world image, arXiv preprint arXiv:2405.17916.
- [41] L. Shan, G. Zhao, J. Xie, P. Cheng, X. Li, Z. Wang, A data-related patch proposal for semantic segmentation of aerial images, *IEEE Geoscience and Remote Sensing Letters* 20 (2023) 1–5.
- [42] G. Zhao, L. Shan, W. Wang, End-to-end remote sensing change detection of unregistered bi-temporal images for natural disasters, in: *International Conference on Artificial Neural Networks*, Springer, 2023, pp. 259–270.
- [43] L. Shan, W. Zhou, W. Li, X. Ding, Lifelong learning and selective forgetting via contrastive strategy, arXiv preprint arXiv:2405.18663.
- [44] L. Shan, S. Luo, Z. Zhu, Y. Yuan, Y. Wu, Cognitive memory in large language models, arXiv preprint arXiv:2504.02441.
- [45] W. Meng, L. Shan, S. Ma, D. Liu, B. Hu, Dlnet: A dual-level network with self-and cross-attention for high-resolution remote sensing segmentation, *Remote Sensing* 17 (7) (2025) 1119.
- [46] B. Du, L. Shan, X. Shao, D. Zhang, X. Wang, J. Wu, Transform dual-branch attention net: Efficient semantic segmentation of ultra-high-resolution remote sensing images, *Remote Sensing* 17 (3) (2025) 540.
- [47] X. Li, L. Shan, W. Wang, Fusing multitask models by recursive least squares, in: *ICASSP 2021-2021 IEEE International Conference on Acoustics, Speech and Signal Processing (ICASSP)*, IEEE, 2021, pp. 3640–3644.
- [48] Y. Ji, L. Shan, Ldnet: Semantic segmentation of high-resolution images via learnable patch proposal and dynamic refinement, in: *2024 IEEE International Conference on Multimedia and Expo (ICME)*, IEEE, 2024, pp. 1–6.
- [49] L. Shan, W. Zhou, W. Li, X. Ding, Organizing background to explore latent classes for incremental few-shot semantic segmentation, arXiv preprint arXiv:2405.19568.
- [50] L. Shan, W. Wang, K. Lv, B. Luo, Edge-guided and class-balanced active learning for semantic segmentation of aerial images, arXiv preprint arXiv:2405.18078.

- [51] X. Ding, L. Shan, G. Zhao, M. Wu, W. Zhou, W. Li, The binary quantized neural network for dense prediction via specially designed upsampling and attention, arXiv preprint arXiv:2405.17776.
- [52] X. Li, L. Shan, M. Li, W. Wang, Energy minimum regularization in continual learning, in: 2020 25th International Conference on Pattern Recognition (ICPR), IEEE, 2021, pp. 6404–6409.
- [53] L. Shan, W. Wang, K. Lv, B. Luo, Boosting semantic segmentation of aerial images via decoupled and multilevel compaction and dispersion, IEEE Transactions on Geoscience and Remote Sensing 61 (2023) 1–16.
- [54] R. Pi, L. Shan, Synthetic lung x-ray generation through cross-attention and affinity transformation, arXiv preprint arXiv:2503.07209.
- [55] X. Zhou, L. Shan, X. Gui, Dynrsl-vlm: Enhancing autonomous driving perception with dynamic resolution vision-language models, arXiv preprint arXiv:2503.11265.
- [56] E. Yi-Ge, L. Shawn, Flexdataset: Crafting annotated dataset generation for diverse applications, in: Proceedings of the AAAI Conference on Artificial Intelligence, Vol. 39, 2025, pp. 9481–9489.
- [57] C. Sun, W. Li, X. Li, Y. Liu, L. Shan, Gmm-based comprehensive feature extraction and relative distance preservation for few-shot cross-modal retrieval, arXiv preprint arXiv:2505.13306.
- [58] H. Luo, B. Wu, H. Jia, Q. Zhu, L. Shan, Llm-cot enhanced graph neural recommendation with harmonized group policy optimization, arXiv preprint arXiv:2505.12396.
- [59] S. Luo, Z. Zhu, Y. Yuan, Y. Yang, L. Shan, Y. Wu, Geogrambench: Benchmarking the geometric program reasoning in modern llms, arXiv preprint arXiv:2505.17653.
- [60] Q. Yi, L. Shan, Geolocsft: Efficient visual geolocation via supervised fine-tuning of multimodal foundation models, arXiv preprint arXiv:2506.01277.
- [61] H. Chen, L. Feng, W. Wu, X. Zhu, S. Leo, K. Hu, F2net: A frequency-fused network for ultra-high resolution remote sensing segmentation, arXiv preprint arXiv:2506.07847.
- [62] L. Mou, Y. Hua, X. X. Zhu, A relation-augmented fully convolutional network for semantic segmentation in aerial scenes, in: The IEEE Conference on Computer Vision and Pattern Recognition (CVPR), 2019.
- [63] K. He, X. Zhang, S. Ren, J. Sun, Deep residual learning for image recognition, in: Proceedings of the IEEE Conference on Computer Vision and Pattern Recognition (CVPR), 2016.

- [64] L. Chen, G. Papandreou, I. Kokkinos, K. Murphy, A. L. Yuille, Semantic image segmentation with deep convolutional nets and fully connected crfs, in: Y. Bengio, Y. LeCun (Eds.), 3rd International Conference on Learning Representations, ICLR 2015, San Diego, CA, USA, May 7-9, 2015, Conference Track Proceedings, 2015.
- [65] X. Pan, J. Shi, P. Luo, X. Wang, X. Tang, Spatial as deep: Spatial cnn for traffic scene understanding, in: Proceedings of the AAAI Conference on Artificial Intelligence, Vol. 32, 2018.
- [66] E. Maggiori, Y. Tarabalka, G. Charpiat, P. Alliez, High-resolution aerial image labeling with convolutional neural networks, IEEE Transactions on Geoscience and Remote Sensing 55 (12) (2017) 7092–7103.
- [67] A. Paszke, A. Chaurasia, S. Kim, E. Culurciello, Enet: A deep neural network architecture for real-time semantic segmentation (2016). [arXiv: 1606.02147](https://arxiv.org/abs/1606.02147).
- [68] M. Oršić, S. Šegvić, Efficient semantic segmentation with pyramidal fusion, Pattern Recognition 110 (2021) 107611.
- [69] G. Lin, A. Milan, C. Shen, I. Reid, Refinenet: Multi-path refinement networks for high-resolution semantic segmentation, in: The IEEE Conference on Computer Vision and Pattern Recognition (CVPR), 2017.
- [70] H. Zhao, J. Shi, X. Qi, X. Wang, J. Jia, Pyramid scene parsing network, in: The IEEE Conference on Computer Vision and Pattern Recognition (CVPR), 2017.